Hydrol. Earth Syst. Sci. Discuss., 9, 1367–1387, 2012
www.hydrol-earth-syst-sci-discuss.net/9/1367/2012/
doi:10.5194/hessd-9-1367-2012

Hydrology and Earth System Sciences Discussions

Electrical capacitance volume tomography of soil water infiltration in a vessel experiments

M. Mukhlisin[1,2], M. R. Baidillah[1], A. El-Shafie[1], M. R. Taha[1], and W. Warsito[3]

[1]Department of Civil and Structural Engineering, Faculty Engineering and Built Environment, Universiti Kebangsaan Malaysia
[2]Department of Civil Engineering, Polytechnic Negeri Semarang, Indonesia
[3]Edwar Technology Co., Tangerang, Banten, Indonesia

Received: 18 January 2012 – Accepted: 18 January 2012 – Published: 26 January 2012

Correspondence to: M. Mukhlisin (mmukhlis2@yahoo.com)

Published by Copernicus Publications on behalf of the European Geosciences Union.

Abstract

Electrical capacitance volume tomography (ECVT) is a recently-developed technique for real-time, non-invasive 3-D monitoring of processes involving materials with strong contrasts in dielectric permittivity. This paper is the first application of the method to visualization of water flow in soil. We describe the principles behind the method, and then demonstrate its use with a simple laboratory infiltration experiment. 32 ECVT sensors were installed on the sides of an empty PVC column. Water was poured into the column at a constant rate, and ECVT data were collected every second. The column was then packed with dry sand and again supplied with water at a constant rate with data collected every second. Data were analyzed to give bulk average water contents, which proved consistent with the water supply rates. Data were also analyzed to give 3-D images (216 voxels) allowing visualization of the water distribution during the experiments. For infiltration into the soil, wall flow, progress of the unstable wetting front, and the final water distribution showing air pockets are clearly visible. Result of this study showed that the normalized dielectric permittivity distribution of the water and the saturated soil is 1.0 and around 0.9, respectively.

1 Introduction

Monitoring water infiltration by using a small soil column experiment is needed to evaluate water flow and solute transport through unsaturated soil. A better understanding of the soil water infiltration process is essential to understand and predict dynamic soil water infiltration and solute transport. However, there are some difficulties with the current techniques for monitoring real time three-dimensional soil water infiltration in unsaturated soil column studies.

To study the underlying physics of water infiltration into unsaturated soil, some methods have been proposed in the past. In general, there are two main methods to study the infiltration of water, i.e. numerical modeling (e.g. Wilkinson et al., 2002; Mukhlisin

HESSD

9, 1367–1387, 2012

et al., 2006, 2008; Liang et al., 2009) and field monitoring (in-situ experiment). In field monitoring experiments, numerous researchers have applied various techniques to monitor soil water infiltration, such as time domain reflectometry (Huisman et al., 2001), disc infiltrometer (Moret and Gonzalez, 2009), microwave radiometer (Jackson et al., 1998), ground penetrating radar (Huisman et al., 2001), and electrical resistance tomography (Brunet et al., 2010; Batlle et al., 2009; Koestel et al., 2009). Although these techniques can generate data by temporal resolution, but the data is still in two-dimensions and only the view data can generate to three-dimensions. Therefore, a monitoring technique that can generate three-dimensional spatial data and real time is still a challenge in the soil-water field.

A well-known noninvasive technique called tomography has been used in many research areas (e.g. medicine, chemical engineering, and geophysics) because it can generate images of internal structures. Recent progress in the development of process tomography has provided in-depth insights into the complex multiphase flow phenomena in many industrial processes (Warsito et al., 2007a). One tomography technique with great potential is electrical capacitance volume tomography (ECVT).

ECVT is a dynamic volume imaging technique that is based on the principle of electrical capacitance tomography (ECT) (Warsito et al., 2007b). This technique is not a post-processing 4D image reconstruction because it creates movie images of electrical permittivity directly from multi-frame volumetric data. This technique has a noninvasive nature and the capability of differentiating between different components based on the permittivity distribution to obtain real time and volumetric (4-D) images of the object (Williams and Beck, 1995). Soil is a mixture of solid, air and water. Because the dielectric constant of water is greater than others, i.e. 81 for frequencies less than 1000 MHz, the value of the dielectric for the soil depends on the water content (Kutilek and Nielsen, 1994). This significant contrast in dielectric properties makes ECVT a great potential tool for monitoring the infiltration of water in soil.

HESSD
9, 1367–1387, 2012

In this study, a small soil column with an ECVT system is developed to monitor water infiltration into an unsaturated soil. This study is the first attempt to apply ECVT to monitor soil water infiltration by real time 3-D imaging.

2 Principle of ECVT

The permittivity distribution is related to the capacitance measurement according to the Poisson equation:

$$\nabla \cdot (\varepsilon(x, y, z)) \nabla \phi(x, y, z) = -\rho(x, y, z), \quad (1)$$

where $\varepsilon(x, y, z)$ is the permittivity distribution, $\phi(x, y, z)$ is the electrical potential distribution and $\rho(x, y, z)$ is the charge distribution.

The mutual capacitance between two pairs of electrodes is given by the ratio between the stored charge and the potential difference:

$$C_{ij} = \frac{Q_{i,j}}{\Delta V_{i,j}} \quad (2)$$

where C_{ij} is the mutual capacitance; $\Delta V_{i,j}$ is the potential difference between electrodes i and j, respectively; and Q_j is the charge on the receiving electrode. Q_j is found by applying Gauss's law:

$$Q_j = \oint_{\Gamma_j} \epsilon(x, y, z) \nabla \phi(x, y, z) \cdot \hat{\boldsymbol{n}} dl, \quad (3)$$

where Γ_j is a closed path that encloses the detecting electrode and $\hat{\boldsymbol{n}}$ is a unit vector normal to Γ_j. Using Eqs. (1) and (3), the mutual capacitance is calculated as follows:

$$C_{i,j} = \frac{1}{\Delta V_{i,j}} \oint_{\Gamma_j} \varepsilon(x, y, z) \nabla \phi(x, y, z) \cdot \hat{\boldsymbol{n}} dl. \quad (4)$$

HESSD
9, 1367–1387, 2012

Thus, the first problem in ECVT is how to measure the capacitance. This is known as the forward problem.

The capacitance value of the medium is measured by using a differential method. This method considers the unknown capacitance to be an element of an active differentiator (Harteveld et al., 1999). The data acquisition system for this task was made by CTech Labs (Edwar Technology Co., Tangerang, Indonesia) and was capable of capturing image data up to 496 independent measurements per 0.25 s.

To perform volumetric imaging, ECVT requires multiple electrodes that are arranged at the boundary of the region. The number of independent measurements depends on the number of electrodes, as described by the following equation:

$$M = ne \cdot (ne - 1)/2, \quad (5)$$

where ne is the number of electrodes. Based on Eq. (4), the ECVT is included in soft field tomography because the relationship between the interrogating field and the permittivity distribution, which is defined by a partial differential equation form, are dependent on each other. Due to the soft field of the electrical field, the capacitance measurement that generates simultaneous information on the volumetric properties can be made by using arbitrary shapes of sensors and vessels (Warsito et al, 2007b). Based on Eq. (4), the measured capacitance depends on the area that encloses the detector electrode. Therefore, the sensitivity of the sensor to differentiate the change in the permittivity value depends on the sensor design. The geometry sensor choice was based on the most optimum geometry to transfer the electrical field. Hexagonal sensors were chosen and are shown in Fig. 1 (left panel); the dimensions of the sensor are depicted in Fig. 1 (right panel).

The components of the sensor are described in detail in Fig. 2. The electrode and ground were composed of copper. The electrode was then linked to a coaxial cable that was used to transfer the measured voltage between the electrode and the ground to the data acquisition system.

Estimating the permittivity distribution from the measured capacitance data is known as the inverse problem. In this step, the sensitivity mode was used to solve the inverse

HESSD
9, 1367–1387, 2012

problem. By using the linearization technique, which is known as the sensitivity model, and by assuming that the permittivity distribution is independent of the electric field distribution, the domain of the system is divided into a number of pixels (see Fig. 3). The linearization form of Eq. (4) is written in the matrix expression as follows:

$$\boldsymbol{C} = \mathbf{S}\,\boldsymbol{G}, \tag{6}$$

where $\boldsymbol{C}$ is a M-dimensional capacitance data vector, $\boldsymbol{G}$ is a N-dimensional image vector, and $\mathbf{S}$ is a $M \times N$ dimensional sensitivity matrix. $M$is the number of electrode-pair combinations (see Eq. 5). N is the number of voxels.

$$N = nx \times ny \times nz, \tag{7}$$

where nx, ny, nz are the number of voxels at the x, y, z axis, respectively. By using a back projection technique, the image vector can be estimated as follows:

$$\boldsymbol{G} = \mathbf{S}^T\,\boldsymbol{C}. \tag{8}$$

The sensitivity matrix $\mathbf{S}$ depends on the geometry of the sensor. Therefore, $\mathbf{S}$ is a unique property of sensors that are capable of differentiating changes in the permittivity distribution. The axial distribution of normalized sensitivity for 496 capacitance pairs is depicted in Fig. 4. The convergence of the iterative reconstruction process is determined by the variation (the difference in the maximum and minimum values in one level) and the smoothness of the slope of the sensitivity distribution curves along the axial direction (Warsito et al., 2007b). In Fig. 4, there are many slope variations in the axial direction. Therefore, an object in almost all of the regions in this sensor will be differentiated. Only in the bottom and upper layers are dead zones found, where there is not much variation. Therefore, convergence towards a solution is difficult in the dead zone area.

Calculation of the sensitivity distribution in this study was based on the equations which can be seen from the previous study (i.e. Lionheart, 2001; Warsito et al., 2007b). Based on this method, the level and distribution of a homogeneous electric field propagation in the area of the object to be measured was affected the sensitivity distribution

HESSD
9, 1367–1387, 2012

of a sensor. In measurement sensitivity distribution, the electric field which propagates through the PVC does not change significantly because permittivity PVC is quite small. Permittivity of air at room temperature is 1 while for the permittivity PVC value between 2.5 to 3. In the reconstruction phase, despite the presence of PVC able to influence the measured capacitance value however this can be eliminated through the calibration process. Calibration process measured the capacitance value at the time of the object area was filled with two medium-low permittivity value (usually air $\varepsilon_r = 1$) and high permittivity value (usually water $\varepsilon_r = 80$). So that the reconstructed capacitance data was the normalized value between the two mediums were used during the calibration process. Thus, the presence of PVC can be ignored.

3 Methodology

Figure 5 shows the experimental setup. The experiment was conducted in a vertical column vessel. The column was 11.5 cm in diameter, 27 cm in height and 3 l in volume. ECVT sensors were attached in the periphery of the vertical column and were composed of 32 electrodes distributed in four planes. All of the sensors were connected to a data acquisition system, and then the data was sent to the PC to be reconstructed.

Before the experiment is conducted, the first step is the calibration process. The purpose of this step is to normalize the capacitance data so that the values ranges between zero and one, see Eq. (9).

In this step, a low-permittivity medium ε_l is defined to be zero in the color scale range (i.e. permittivity of air), while a high-permittivity medium ε_h is defined to be one (i.e. permittivity of water). The normalized capacitance is expressed as follows:

$$C_{i,j} = \frac{C_{m(i,j)} - C_{l(i,j)}}{C_{h(i,j)} - C_{l(i,j)}}, \quad (9)$$

($i = 1 \ldots ne$, $j = i + 1 \ldots ne$), where $C_{i,j}$ is the normalized capacitance of the electrode pair $i - j$, $C_{m(i,j)}$ is the measured capacitance of the electrode pair $i - j$, and $C_{l(i,j)}$,

HESSD
9, 1367–1387, 2012

$C_{h(i,j)}$ are the capacitances of the electrode with the function ε_l and ε_h, respectively. The image is reconstructed with a resolution of $32 \times 32 \times 32$ based on iterative linear back propagation (ILBP). The relationship between the pixel size and the real size in the vessel can be seen in Fig. 3. The pixel lengths *nx*, *ny*, *nz* are 0.358 cm, 0.358 cm, and 0.84 cm, respectively. Therefore, the voxel volume is about 0.11 cm^3.

In this study, two experimental procedures were conducted. The first procedure was implemented by supplying water to the empty vessel; the second procedure was applied by filling the vessel with soil and then gradually filling the soil column with water. To test the image reconstruction performance of ECVTs that are capable of detecting the change in water content, experiment 1 was conducted first. In this experiment, the empty column with air as the background medium was filled with water. The water volume was increased by supplying a water discharge of 6 ml s^{-1}. In this experiment, air was the low permittivity medium ε_l, and water was the high permittivity medium ε_h.

For the second experiment, 3 l by volume of soil in the vessel was supplied. The soil material that was used in this study was sand collected from the Cisadane river in Tangerang, Indonesia. The soil contained 17 % fine sand and 83 % medium sand. The specific gravity and soil density were 2.663 and 1.55 g cm^{-3}, respectively.

In this experiment, the soil in the vessel was supplied with water flow with a discharge 7.2 ml s^{-1} until ponded condition and maintained the pond of water level at 2 cm above the surface soil. During ponded condition, the data capacitances were measured iteratively and sent to the computer. The data acquisition frequency was set to one frame per second. In this experiment, the dry soil acted as the low permittivity medium ε_l, while pure water was the high permittivity medium ε_h.

HESSD
9, 1367–1387, 2012

4 Results and discussion

4.1 Imaging of 3-D water flow in the vessel

Figures 6 and 8 show the reconstructed image data by using ILBP as the image reconstruction algorithm, which took 10 iterations to inverse the data. From the first experiment, the behavior of the ECVT system can be seen when the medium was filled with water continuously. Figure 6a shows the background medium in which air was filled by water flow. The increasing water content in the vessel can be seen by increasing the red color in the medium (see Fig. 6b to l). The figure shows that water filled up to half of the vessel at 300 s, and the water almost filled up the vessel at 500 s. Vertical yellow color in the figure reflected a water flowing in the vessel, while horizontal yellow color in water surface is affected by boundary interaction between the permittivity of water and air. The reconstructed image of increasing water flow in the vessel can be well illustrated second by second in this study.

Figure 6a to l are representative of the normalized capacitance from 12 different frames. In each frame, 496 simultaneous measurements can be estimated for one second of acquisition. Figure 7 shows the normalized mean capacitance value for all of the data at each frame, where the values of 0 and 1 illustrate empty and full water in the vessel, respectively. Increasing the water content in the vessel resulted in an increase in the normalized mean capacitance value as well. From this figure, it can be seen that the value of the mean normalized capacitance per frame starts to increase at around 100 s and continues to increase until around 500 s. The value of the mean normalized capacitance was steady at level 1 from 500 s to 600 s, which means that the water was full in the vessel (see Figs. 6 and 7).

HESSD
9, 1367–1387, 2012

4.2 Imaging of 3-D soil water infiltration

Figure 8 shows images of soil water infiltration in twelve different time segments. The color bar scale from 0 to 1 indicates the value of the normalized permittivity. The blue color indicates that the medium is a fully low permittivity medium (i.e. dry soil), while the red shade indicates a high permittivity medium (i.e. saturated soil water content). The figure illustrates the pattern of soil water infiltration in the vessel. Although the water was supplied from the top at a central point in the vessel, the water tends to infiltrate the soil from the edge of the vessel; then, the soil water infiltrated up to half of the vessel around 350 s. At the end of the experiment, some blue-colored regions were observed in the bottom part of the vessel. This was potentially due to air traps that stop water infiltration in this area.

Figure 9 shows the mean normalized capacitance for 1000 frames. This figure shows that the value of the mean normalized capacitance in the system was 0 for dry soil conditions, while for saturated soil, the value was around 0.9. Increasing water infiltration in the soil resulted in an increase in the mean normalized capacitance. When the soil is saturated, the permittivity will not be as high as pure water. Therefore, the value of the mean normalized capacitance and the color bar in Figs. 8 and 9 will not reach the pure water value.

5 Conclusions

Monitoring of water flow and soil water infiltration by using a tomography technique in unsaturated soil has been conducted in this study. The system has successfully reconstructed real time 3-D images of water flow and soil water infiltration in a vessel (vertical soil column). The real time images of the increasing water level in the vessel were monitored very well. In addition, this study has also successfully monitored water infiltration in unsaturated soil. Both of the experiments can be entirely monitored because the system can determine differences in the normalized dielectric permittivity

HESSD
9, 1367–1387, 2012

distribution between the water and the saturated soil, which is 1.0 and around 0.9, respectively. The system was also successful in real time 3-D imaging of the qualitative soil moisture content, as shown in the color scale range. This study shows that ECVT is a potential tool for monitoring real time processes in soil-water sciences.

Supplementary material related to this article is available online at: http://www.hydrol-earth-syst-sci-discuss.net/9/1367/2012/hessd-9-1367-2012-supplement.zip.

Acknowledgements. This work was supported by grant from the Ministry of Science, Technology and Innovation (MOSTI) of Malaysia and Fundamental Research Grant Scheme (FRGS) under Ministry of Higher Education (MOHE) of Malaysia.

References

Batlle-Aguilar, J., Pessel, M., Tucholka, P., Coquet, Y., and Vachier, P.: Axisymetrical Infiltration in Soil Imaged by Noninvasive Electrical Resistivimetry, Soil Sci. Soc. Am. J., 73, 510–520, 2009.

Brunet, P., Clement, R., and Bouvier, C.: Monitoring soil water content and deficit using Electrical Resistivity Tomography (ERT) – A case study in the Cevennes area, France, 146–153, 2010.

Harteveld, W. K., van Halderen, P. A., Mudde, R. F., van den Bleek, C. M., van den Akker, H. E. A., and Scarlett, B.: A fast active differentiator capacitance transducer for electrical capacitance tomography, 1st Word Congress on Industrial Process Tomography, Buxton, Greater, Manchester, 14–17 April, 564–567, 1999.

Huisman, J., Sperl, C., Bouten, W., and Verstraten, J.: Soil water content measurements at different scales: accuracy of time domain reflectometry and ground-penetrating radar, J. Hydrol., 245, 48-58, 2001.

Jackson, T. J., Schmugge, T. J., and Rawls, W. J.: soil water infiltration observation with microwave radiometers, IEEE T. Geosci. Remote, 36, 1376-1383, 1998.

HESSD

9, 1367–1387, 2012

Koestel, J., Kasteel, R., Kemna, A., Esser, O., Javaux, M., Binley, A., and Vereecken, H.: Imaging Brilliant Blue Stained Soil by Means of Electrical Resistivity Tomography, Vadose Zone J., 8, 963–975, 2009.

Liang, W. L., Kosugi, K., and Mizuyama, T.: A three-dimensional model of the effect of stemflow on soil water dynamics around a tree on a hillslope, J. Hydrol., 366, 62–75, 2009.

Lionheart, W. R. B.: Reconstruction algorithms for permittivity and conductivity imaging, in: Proc. 2nd World Congr. Industrial Process Tomography, Hannover, Germany, 4–11, 2001.

Moret, D. and Gonzalez, C.: New method for monitoring soil water infiltration rates applied to a disc infiltrometer, J. Hydrol., 379, 315-322, 2009.

Mukhlisin, M., Kosugi, K., Satofuka, Y., and Mizuyama, T.: Effects of Soil Porosity on Slope Stability and Debris Flow Runout at a Weathered Granitic Hillslope, Vadoze Zone J., 5, 283–295, 2006.

Mukhlisin, M., Taha, M. R., and Kosugi, K.: Numerical analysis of effective soil porosity and soil thickness effects on slope stability at a hillslope of weathered granitic soil formation, Geosci. J., 12, 401–410, 2008.

Warsito, W., Marashdeh, Q., and Fan, L.: Real time volumetric imaging of multiphase flows using Electrical Capacitance Volume-Tomography (ECVT), 5th World Congress on Industrial Process Tomography, Bergen, Norway, 2007a.

Warsito, W., Marashdeh, Q., and Fan, L.-S.: Electrical Capacitance Volume Tomography, IEEE Sensors J., 7, 525-535, 2007b.

Wilkinson, P. L., Anderson, M. G., and Lloyd, D. M.: An Integrated hydrological model for rain-induced landslide prediction, Earth Surf. Proc. Land., 27, 1285–1297, 2002.

HESSD

9, 1367–1387, 2012

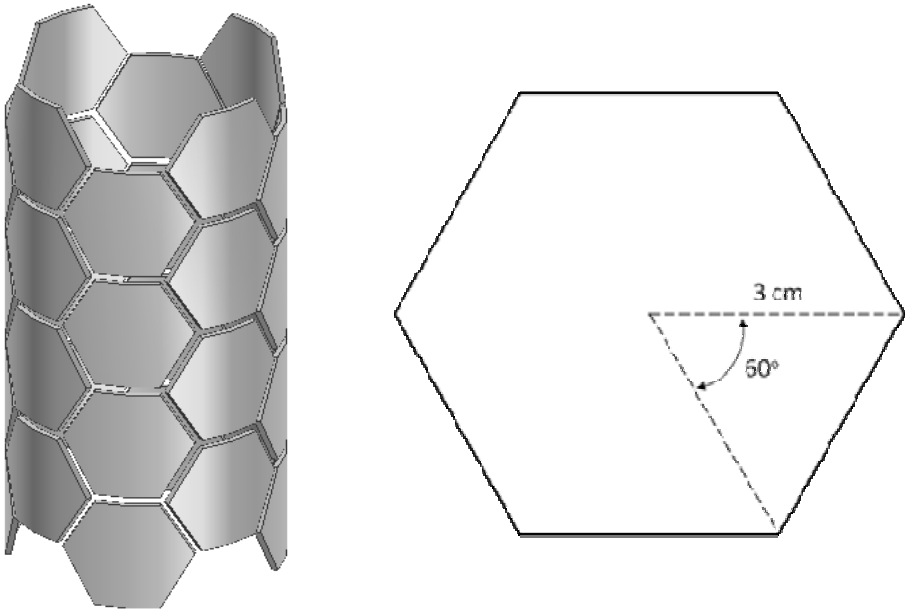

Fig. 1. Left panel: the geometry of the ECVT sensor; right panel: the sensor's dimensions.

HESSD
9, 1367–1387, 2012

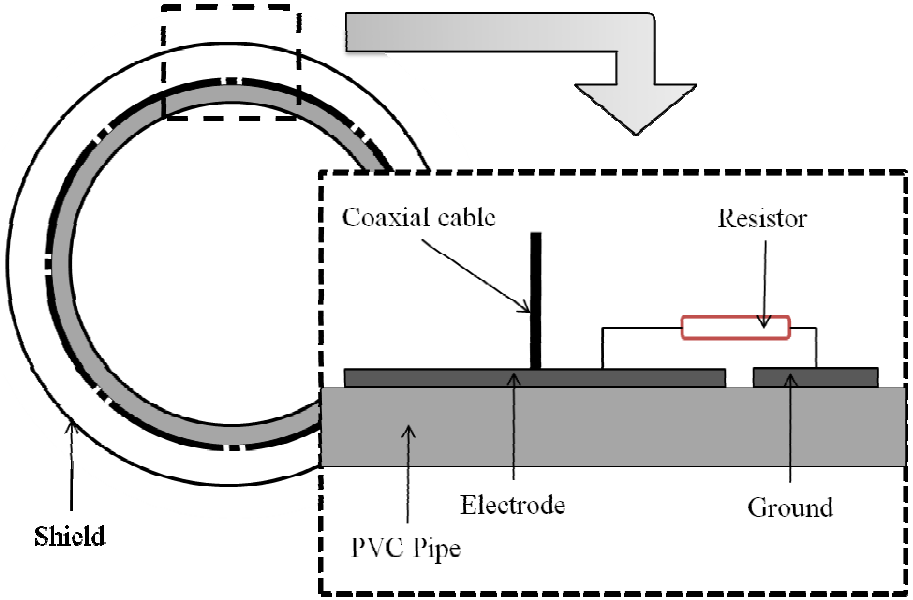

Fig. 2. Details of the ECVT sensor.

HESSD
9, 1367–1387, 2012

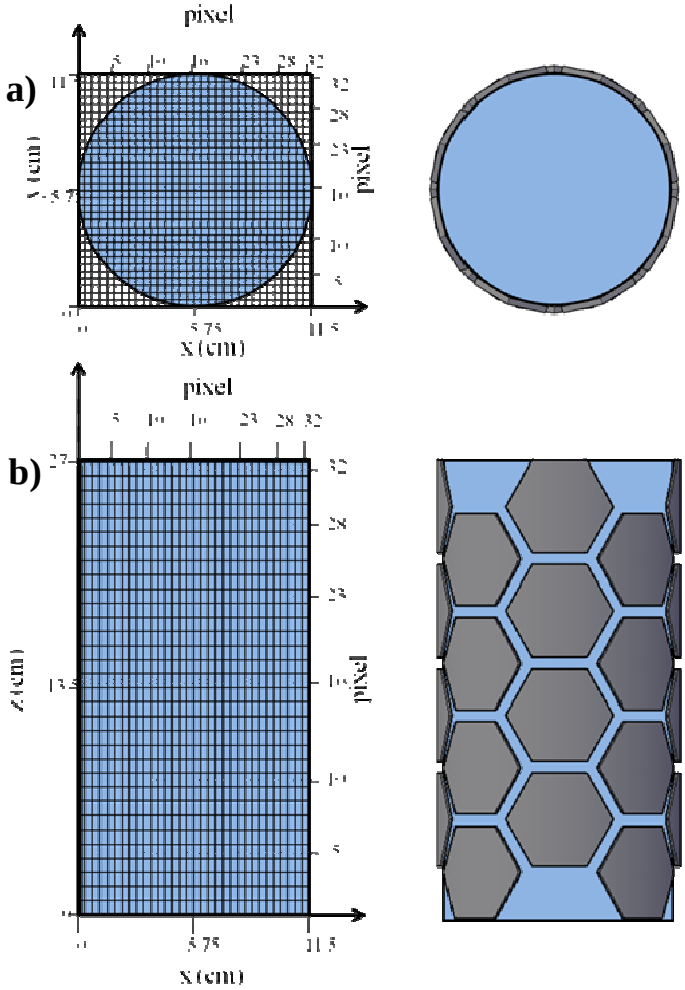

Fig. 3. (a) Top and **(b)** front views of the number of pixels and the vessel.

HESSD
9, 1367–1387, 2012

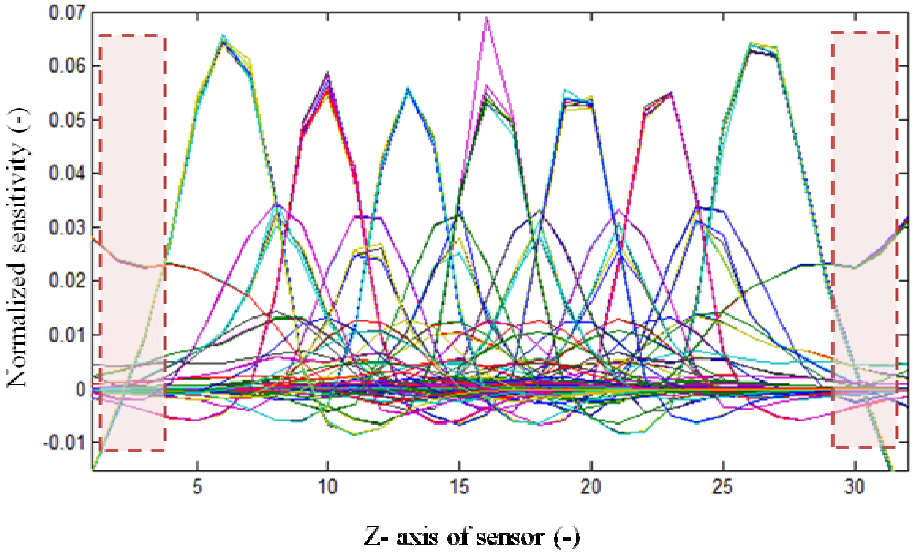

Fig. 4. Sensitivity matrix curve for the hexagonal sensor. The dead zone area is indicated by the dashed line areas.

HESSD
9, 1367–1387, 2012

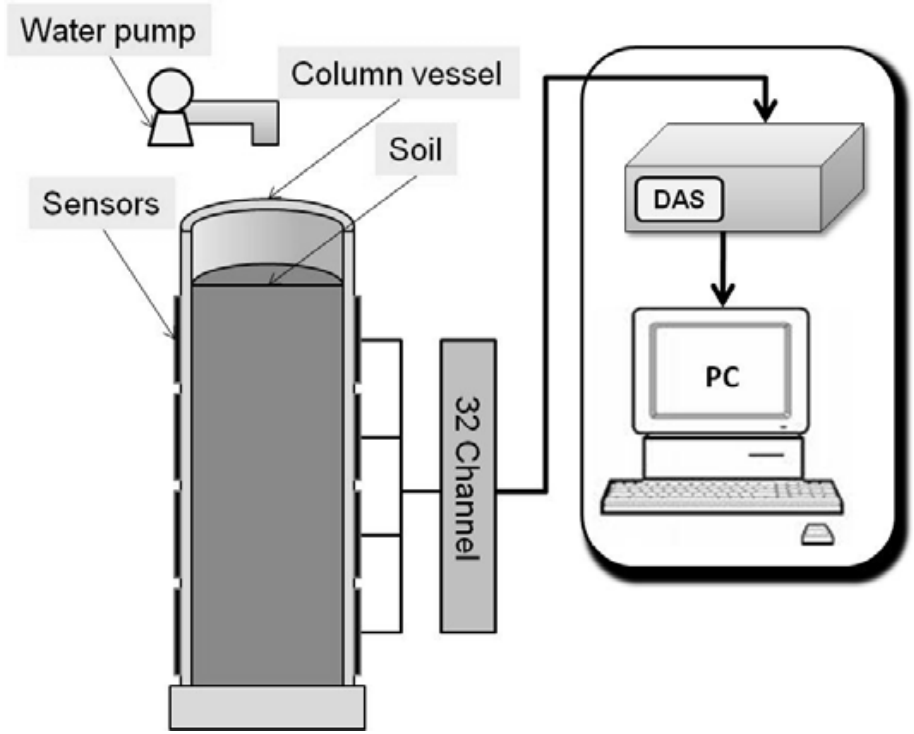

Fig. 5. Sketch of the ECVT system.

HESSD
9, 1367–1387, 2012

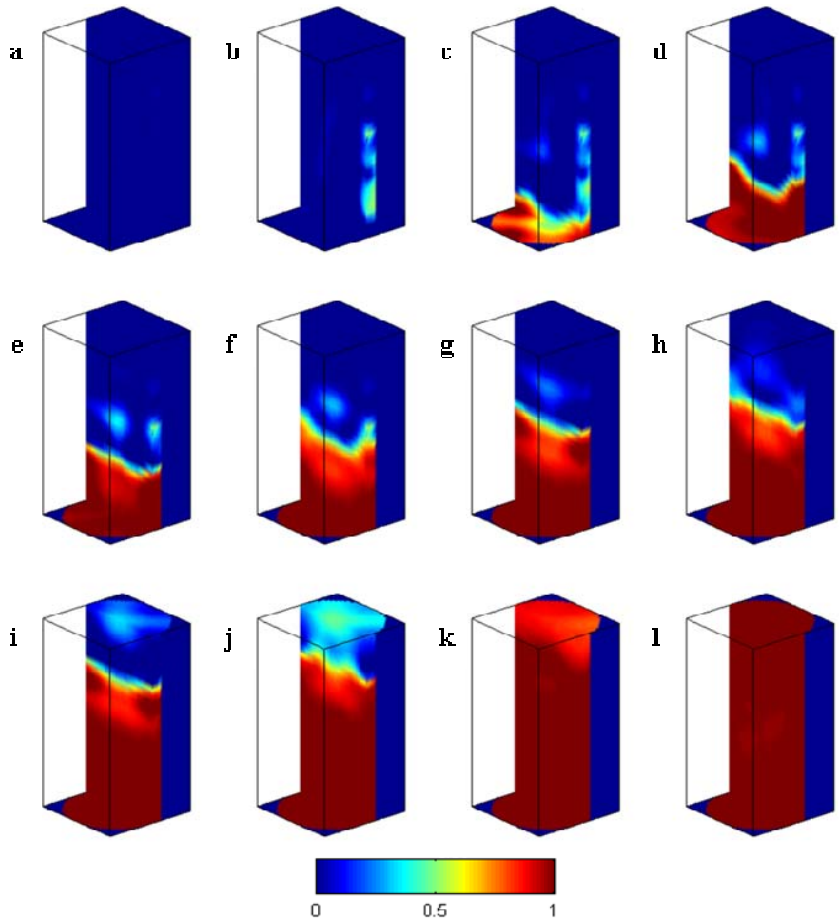

Fig. 6. Permittivity distribution of the water at time **(a)** 1 s, **(b)** 50 s, **(c)** 100 s, **(d)** 150 s, **(e)** 200 s, **(f)** 250 s, **(g)** 300 s, **(h)** 350 s, **(i)** 400 s, **(j)** 450 s, **(k)** 500 s, and **(l)** 550 s.

HESSD
9, 1367–1387, 2012

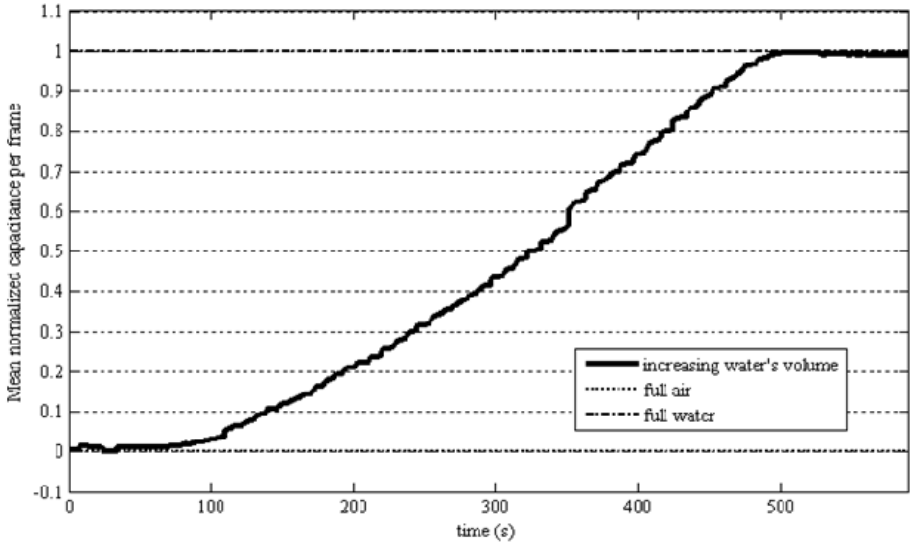

Fig. 7. Mean normalized capacitance per frame for the air-water calibration.

HESSD
9, 1367–1387, 2012

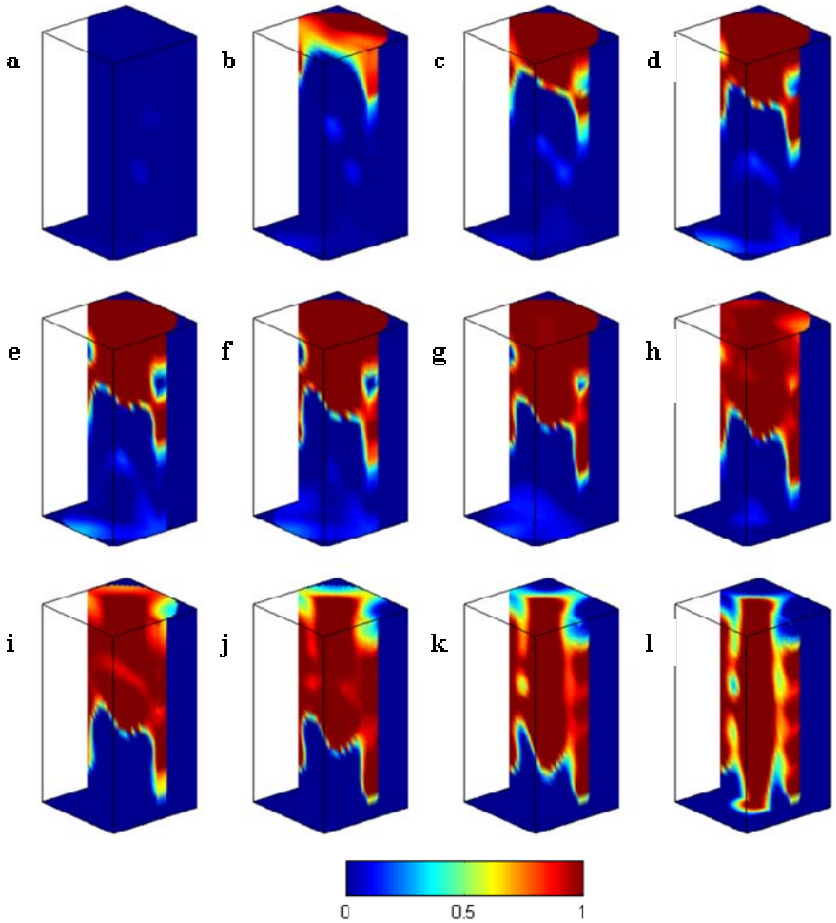

Fig. 8. Permittivity distribution of the soil water infiltration at time **(a)** 1 s, **(b)** 50 s, **(c)** 100 s, **(d)** 150 s, **(e)** 200 s, **(f)** 250 s, **(g)** 300 s, **(h)** 350 s, **(i)** 400 s, **(j)** 500 s, **(k)** 600 s, and **(l)** 700 s.

HESSD
9, 1367–1387, 2012

Electrical capacitance volume tomography of soil water infiltration

M. Mukhlisin et al.

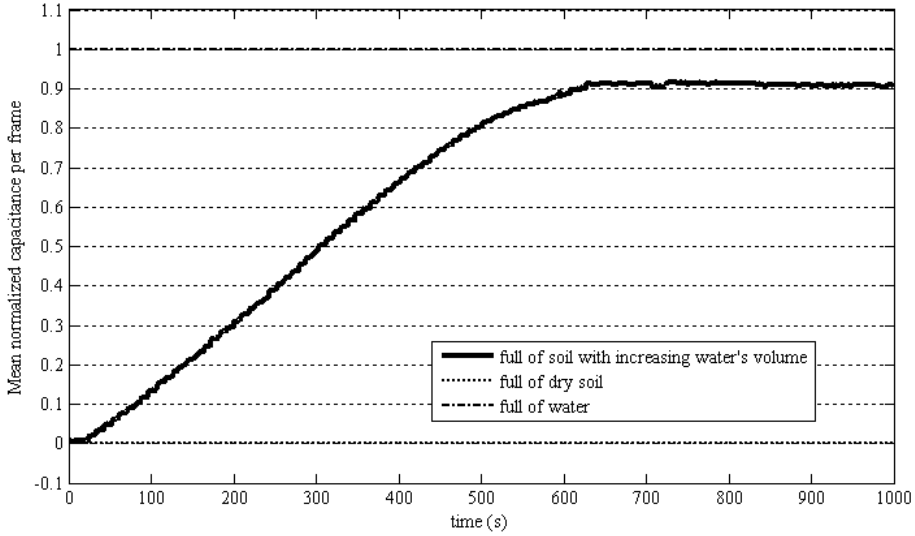

Fig. 9. Mean normalized capacitance per frame for the dry soil-water calibration.

HESSD
9, 1367–1387, 2012